

ChemComm

Accepted Manuscript



This is an *Accepted Manuscript*, which has been through the Royal Society of Chemistry peer review process and has been accepted for publication.

Accepted Manuscripts are published online shortly after acceptance, before technical editing, formatting and proof reading. Using this free service, authors can make their results available to the community, in citable form, before we publish the edited article. We will replace this *Accepted Manuscript* with the edited and formatted *Advance Article* as soon as it is available.

You can find more information about *Accepted Manuscripts* in the [Information for Authors](#).

Please note that technical editing may introduce minor changes to the text and/or graphics, which may alter content. The journal's standard [Terms & Conditions](#) and the [Ethical guidelines](#) still apply. In no event shall the Royal Society of Chemistry be held responsible for any errors or omissions in this *Accepted Manuscript* or any consequences arising from the use of any information it contains.



Journal Name

COMMUNICATION

Synthesis of Dendritic Pt-Ni-P Alloy Nanoparticles with Enhanced Electrocatalytic Properties

Received 00th January 20xx,
Accepted 00th January 20xx

Jingfang Zhang, Kaidan Li, Bin Zhang*

DOI: 10.1039/x0xx00000x

www.rsc.org/

Dendritic Pt-Ni-P alloy NPs with different chemical compositions were successfully synthesized via a facile wet-chemical route. Owing to the unique dendritic nanostructures and synergistic electronic effects of P, Ni, and Pt atoms, the as-prepared dendritic Pt-Ni-P alloy NPs exhibit higher electrocatalytic activity over dendritic Pt-Ni alloy NPs and commercial Pt/C.

The Exploitation of efficient and economically viable energy conversion technologies have attracted much research interest as promising candidates to replace combustion-based energy sources.¹ Low temperature fuel cells, especially small organic molecules (e.g., methanol, formic acid) as renewable fuels, are among the most potential power sources for automotive vehicles and portable electronic devices.² Specifically, direct methanol fuel cells (DMFCs) and direct formic acid fuel cells (DFAFCs) have many advantages, such as satisfactory energy density at low temperature, low pollutant emission, easy storage and transportation.³ Typically, platinum (Pt), as the most efficient electrocatalyst that are utilized at anodes for methanol oxidation reaction (MOR) and formic acid oxidation reaction (FAOR), has been extensively studied. However, there are a number of obstacles including the high cost, the insufficient activity, and the surface poisoning by carbonaceous species generated in the reaction of the Pt catalysts.⁴ These shortcomings inevitably lead to sluggish kinetics and low efficiency, which highlights the need for the development of more active and durable anode catalysts with largely decreasing the loading of Pt.⁵

One effective strategy to solve these problems is incorporating the 3d-transition metals (M = Fe, Co, Ni, V, Ti) into pure Pt nanostructures. The resulted Pt-M alloys exhibit outstanding electrocatalytic performance mainly due to the ligand and synergistic effects between the different components.⁶ Moreover, the doping of non-metallic element phosphorus (P) with abun-

dant valence electrons has been proved to modulate the electronic structure of metal elements, thus enhancing the electrocatalytic activity.⁷ Therefore, the development of P-doped Pt-based ternary composite electrocatalysts is one of the key topics of frontier research.⁸

Pt-based nanostructures with well-controlled shape are interesting materials for innovative catalyst design with improved physical and chemical properties.⁹ Dendritic nanostructures are expected to show substantially excellent properties,¹⁰ due to their open structures, rich edges and corner atoms, as well as large surface area accessible to the reactant molecules.¹¹ However, to date, the development of a facile and general synthetic methodology to prepare the dendritic P-doped Pt-based ternary nanostructures with high electrocatalytic activity, is still highly desirable.

Herein, we report a one-pot wet-chemical synthetic strategy to fabricate novel dendritic Pt-Ni-P alloy nanoparticles (NPs) with very thin branches (~3 nm) as subunits. The dendritic Pt-Ni-P alloy NPs exhibit higher specific and mass activities towards MOR and FAOR in compared with binary dendritic Pt-Ni alloy NPs and commercial Pt/C. The synthesis on this new class of P-doped dendritic catalysts can be reasonably sustainably produced on a large-scale because it is environmentally achieved in aqueous-phase at room temperature.

The dendritic Pt-Ni-P alloy NPs were prepared by using a one-pot wet-chemical route in aqueous solutions involving Pluronic F68, K₂PtCl₆, NiCl₂, and NaH₂PO₂. The as-prepared products were initially examined by scanning electron microscopy (SEM) and transmission electron microscopy (TEM). As shown in Figure 1a, the products consist of highly monodispersed roughly spherical shape. As shown in Figure 1b, well-defined dendritic nanostructures with an average diameter of 41 nm were observed. These dendritic spheres consist of a number of interconnected branches with a width of about 3 nm (Figure S1). Remarkably, these nanobranches were grown in various directions, thus creating an open structure. The structure of the as-prepared samples is characterized by high-magnification TEM (HRTEM) and selected area electron diffraction (SAED). From Figure 1c, we can see abundant defects (e.g.,

Department of Chemistry, School of Science, Tianjin University, and Collaborative Innovation Center of Chemical Science and Engineering (Tianjin), Tianjin 300072, China. E-mail: bzhang@tju.edu.cn

*Electronic Supplementary Information (ESI) available: Experimental section and characterization results. See DOI: 10.1039/x0xx00000x

atomic steps/corners) exist on surfaces of the branches, which can act as highly active sites for electrocatalysis.^{7c,12} And Figure

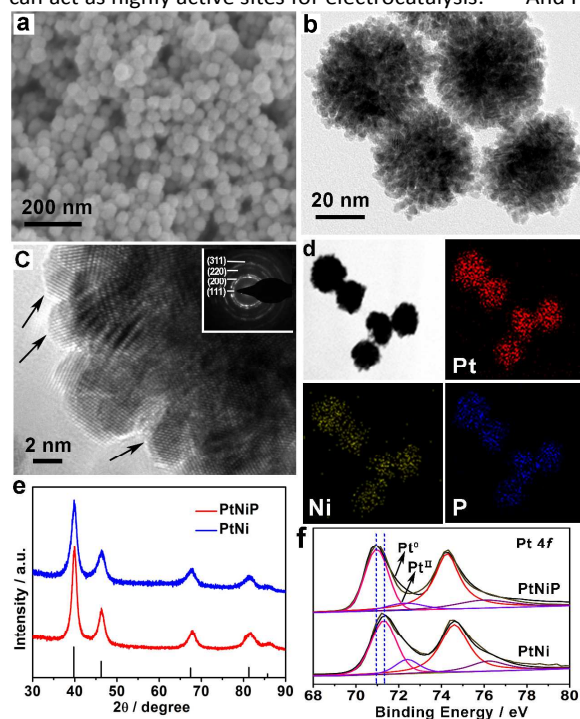


Figure 1. (a-c) SEM image (a), TEM image (b), HRTEM images (c) and the associated SAED pattern (inset in c) of dendritic Pt-Ni-P NPs. The atomic steps/corners on the branch are indicated by black arrows. (d) The corresponding TEM image and elemental mapping images showing the distribution of Pt, Ni and P. (e, f) XRD patterns (e) and XPS spectra of the Pt 4f region (f) for dendritic Pt-Ni-P and Pt-Ni NPs.

1c reveals a highly ordered fringe pattern of each individual crystallite segment, but different lattice orientations can be observed from the overall dendritic nanostructures.¹³ Also, the concentric ring patterns with discrete diffraction spots in the SAED pattern (inset of Figure 1c), which can be indexed to the crystal planes of face-centered cubic (fcc) Pt, indicate the polycrystalline character of the dendritic nanostructures. The energy dispersive X-ray (EDX) spectrum (Figure S2) reveals that the NPs are composed of Pt, Ni and P. Quantitative analysis from EDX shows 66.85 at% Pt, 6.56 at% Ni, and 26.59 at% P in the dendritic Pt-Ni-P NPs (almost same with ICP-MS result: 64.57 at% Pt, 6.57 at% Ni, and 28.86 at% P). The EDX elemental mapping images (Figure 1d) confirm that Pt, Ni and P are distributed uniformly throughout the entire dendritic NPs. For comparison, dendritic Pt-Ni NPs were also synthesized in the absence of NaH_2PO_2 with other conditions unchanged (Figure S3). The chemical composition of dendritic Pt-Ni NPs is 90.92 at% Pt and 9.08 at% Ni by ICP-MS. X-ray diffraction (XRD) analysis was employed to characterize the crystalline phase of the dendritic Pt-Ni-P and Pt-Ni NPs (Figure 1e). The peaks observed for both of the two samples can be ascribed to the corresponding (111), (200), (220), (311) and (222) planes of an underlying fcc Pt structure (JCPDS no. 04-0802) without apparent peaks indexed to other impurities within the NPs. Moreover, each of the peaks shifts to higher 2θ values compared to

pure Pt, further indicating the formation of uniform alloy structures. Specific peak positions were collected from the XRD data (Table S2). From Table S2, we have noticed the 2θ values of dendritic Pt-Ni NPs increase compared with the pure Pt, in which Pt lattice contraction occurs as a result of the partial substitution of larger Pt atoms by smaller Ni atoms. For dendritic Pt-Ni-P NPs, the 2θ values decrease compared with the dendritic Pt-Ni NPs, implying Pt-Ni lattice expands by the incorporation of P atoms.¹⁴ Time-resolved TEM images were used to elucidate the morphological evolution of the dendritic Pt-Ni-P NPs, as shown in Figure S4. Dendritic Pt NPs are firstly obtained in a simple reaction system at $t = 4$ h (Figure S4a). During the NPs growth, Pluronic F68 surfactant serves as a structure-directing agent (Figure S5). The Pluronic groups can be easily absorbed on the deposited Pt surface, leading to the dendritic Pt formation.^{10b,c} Afterwards, the NPs started to grow upon the addition of NaBH_4 in the reaction system involving NiCl_2 , NaH_2PO_2 and the unreacted K_2PtCl_4 solution according to the seed-mediated co-reduction mechanism.^{9e}

The surface composition of dendritic Pt-Ni-P NPs was further analyzed by X-ray photoelectron spectroscopy (XPS). Figure 1f shows XPS spectra of the Pt 4f region for dendritic Pt-Ni-P and Pt-Ni NPs. Each Pt 4f peak can be fitted to two pairs of doublets with a spin-orbit separation. The two peaks located at 74.2 eV and 70.9 eV of dendritic Pt-Ni-P NPs could be assigned to elemental $\text{Pt}^0 4f_{5/2}$ and $\text{Pt}^0 4f_{7/2}$, respectively.¹⁵ And a small percentage of Pt^{II} also exists in dendritic Pt-Ni-P NPs. In addition, the slight negative shift in the binding energies compared to that of dendritic Pt-Ni NPs ($\text{Pt} 4f_{7/2}$, 71.3 eV) suggests a decrease of d-electron density of Pt modified by Ni and P and thus an appearance of d-band vacancies within dendritic Pt-Ni-P alloy NPs, which are beneficial for high electrocatalytic activity.¹⁶ A positive shift can be also seen in P 2p spectrum (Figure S6). All these results provide strong evidence for the electron interactions of P, Ni, and Pt atoms in the alloy structure of the dendritic Pt-Ni-P NPs.

Motivated by the unique dendritic structure of the Pt-Ni-P NPs, we chose MOR as a model platform to examine the composition-dependent activity (Table S3 and Figure S7, S8). From

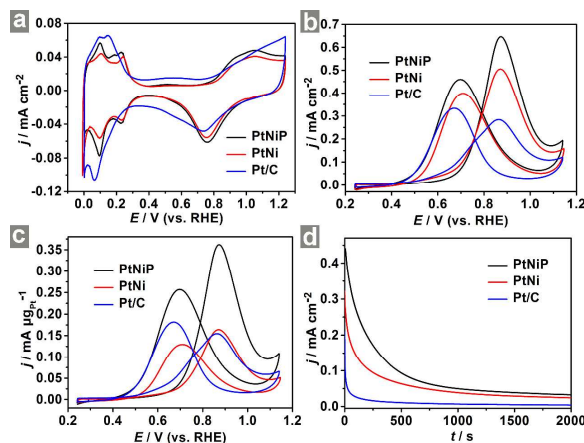


Figure 2. (a) CVs of as-prepared dendritic Pt-Ni-P alloy NPs, dendritic Pt-Ni alloy NPs, and commercial Pt/C in an N_2 -purged solution of 0.5 M H_2SO_4 at a scan rate of 50 mV s^{-1} . (b, c) Specific activities (b), mass activities (c) of MOR recorded in 0.5 M $\text{H}_2\text{SO}_4 + 0.5$

M CH₃OH solution at a scan rate of 50 mV s⁻¹. (d) Chronoamperometry curves of the three catalysts in 0.5 M H₂SO₄ + 0.5 M CH₃OH solution at 0.79 V.

these data, we demonstrated that amounts of Ni and P by alloying with Pt have an important effect on electrocatalytic performance. So the dendritic Pt-Ni-P alloy NPs catalyst with optimized atomic ratio (66.85 at% Pt, 6.56 at% Ni, and 26.59 at% P) was determined as the best electrocatalyst among the five selected samples.

The dendritic Pt-Ni-P alloy NPs (our sample) as typical catalyst was used to investigate and correlate the impact of doping P on electrochemical performance for MOR and FAOR. For comparison, dendritic Pt-Ni alloy NPs and commercial Pt/C were measured. The electrochemically active surface areas (ECSAs) were calculated from integrated H_{upd} region and CO stripping (Table S4). Considering that the ECSA_{CO}/ECSA_H ratio (1:1) and the popularity of H_{upd} method, the specific current density was normalized to the ECSA_H measured by the H_{upd} adsorption method.¹⁷ According to the cyclic voltammograms (CVs) shown in Figure 2a, the positions of the oxide reduction peaks of dendritic Pt-Ni-P and Pt-Ni alloy NPs have positive shifts relative to commercial Pt/C. This observation may be ascribed to the weakening interaction with the oxide species adsorbed on surface because of ligand effect caused by the doping of Ni and P.^{13,18}

Figure 2b and c exhibit the specific and mass activities of MOR recorded in 0.5 M H₂SO₄ + 0.5 M CH₃OH solution at 50 mV s⁻¹. For specific activities, the peak current density of MOR on dendritic Pt-Ni-P alloy NPs (0.65 mA cm⁻²) is 1.3 and 2.3 times than that of dendritic Pt-Ni alloy NPs (0.51 mA cm⁻²) and Pt/C (0.28 mA cm⁻²), respectively, in spite of the lower loading amount of Pt on working electrode. Meanwhile, the corresponding mass activities of three catalysts were also tested. The peak current density on dendritic Pt-Ni-P alloy NPs (0.36 mA μg_{Pt}⁻¹) is 2.1 and 2.4 times that of dendritic Pt-Ni alloy NPs (0.17 mA μg_{Pt}⁻¹) and Pt/C (0.15 mA μg_{Pt}⁻¹), respectively. It is evident that dendritic Pt-Ni-P alloy NPs exhibits markedly enhanced electrocatalytic activity compared with dendritic Pt-Ni alloy NPs and Pt/C. In addition, the peak current ratio of the forward to backward scans, that is, (*j_f/j_b*), can be used to evaluate the poisoning tolerance of catalysts to carbonaceous species in MOR.¹⁹ The *j_f/j_b* ratio of the as-prepared dendritic Pt-Ni-P alloy NPs (1.4) is larger than that of dendritic Pt-Ni alloy NPs (1.3) and Pt/C (0.85), respectively. It means that dendritic Pt-Ni-P alloy NPs catalyst has a lower poisoning susceptibility. As indicated by chronoamperometry curves for 2000 s (Figure 2d), dendritic Pt-Ni-P alloy NPs catalyst also exhibits higher specific current densities and a slower current decay than that of dendritic Pt-Ni alloy NPs and Pt/C during the entire process, demonstrating that dendritic Pt-Ni-P NPs catalyst is more electroactive for MOR and a better tolerance to poisoning carbonaceous species generated in MOR, thus indicative of good stability in MOR. More importantly, further electrochemical measurement of the FAOR (Figures 3a and b) indicated that the specific activities (mass activities) of dendritic Pt-Ni-P alloy NPs (1.04 mA cm⁻²) (0.56 mA μg_{Pt}⁻¹) is 1.3 (2.2) and 2.7 (2.5) times that of dendritic Pt-Ni alloy NPs (0.80 mA cm⁻²) (0.26 mA

μg_{Pt}⁻¹) and Pt/C (0.39 mA cm⁻²) (0.22 mA μg_{Pt}⁻¹), respectively. The dendritic Pt-Ni-P NPs also demonstrated better stability in the FAOR by chronoamperometry curves for 6000 s (Figure 3c).

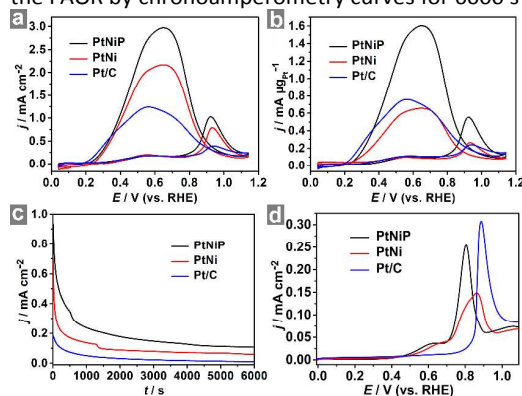


Figure 3. (a, b) Specific activities (a), mass activities (b) of FAOR for dendritic Pt-Ni-P alloy NPs, dendritic Pt-Ni alloy NPs, and commercial Pt/C recorded in 0.5 M H₂SO₄ + 0.5 M HCOOH solution at 50 mV s⁻¹. (c) Chronoamperometry curves of the three catalysts in 0.5 M H₂SO₄ + 0.5 M HCOOH solution at 0.89 V. (d) Representative CO stripping curves for the three catalysts in 0.5 M H₂SO₄ solution at 50 mV s⁻¹.

CO stripping curves (Figure 3d) were recorded to probe the CO tolerance of catalysts. The curves in hydrogen desorption region between -0.01 and 0.34 V are in straight lines owing to the coverage of adsorbed CO on the Pt active sites.²⁰ As observed in Figure 3d, the peak potential (0.80 V) of CO oxidation on the dendritic Pt-Ni-P alloy NPs is obviously more negative than that of the dendritic Pt-Ni alloy NPs (0.86 V) and commercial Pt/C (0.89 V). This reveals that dendritic Pt-Ni-P alloy NPs have the best CO removal ability, which might arise mainly from the doping of Ni and P lowering the d-band center of the Pt, thus weakening the absorption strength of CO with Pt active sites and improving the electroactivity.^{16,18}

We also evaluated the electrochemical durability of the dendritic Pt-Ni-P alloy NPs by prolonged cycles between 0 and 1.24 V in 0.5 M H₂SO₄ at 50 mV s⁻¹. As shown in Figure S9a and S9b, the CV measurements show a loss of 22.5% in ECSA for dendritic Pt-Ni-P alloy NPs, 36.6% for dendritic Pt-Ni alloy NPs and 49.9% for commercial Pt/C after 1500 potential cycles, revealing that the durability of dendritic Pt-Ni-P alloy NPs is also better than dendritic Pt-Ni alloy NPs and commercial Pt/C. The morphologies of these electrocatalysts after durability tests were also examined by TEM (Figures S9c-f). While serious aggregation and falling off of Pt are observed for commercial Pt/C, Pt-Ni-P and Pt-Ni alloy NPs retain the well-defined dendritic morphology. These results indicate that dendritic Pt-Ni-P NPs have a superior catalytic activity and durability than dendritic Pt-Ni NPs and commercial Pt/C. The enhanced performance of dendritic Pt-Ni-P alloy NPs should due to the following reasons: 1) the high ECSA and abundant accessible atomic steps/corners as active sites provided by the unique dendritic nanostructures; 2) the stable nanostructure consisting of many thin branches, less vulnerable to Ostwald ripening, and aggregation;^{5a} 3) the synergetic effects among Pt, Ni, and P.

In summary, we demonstrate a facile wet-chemical approach to the composition-controlled dendritic Pt-Ni-P alloy

NPs with very thin branches as subunits. The dendritic Pt-Ni-P alloy NPs exhibit superior structural stability and enhanced, composition-dependent electrocatalytic activity toward both MOR and FAOR over dendritic Pt-Ni alloy NPs and commercially Pt/C catalysts. It is found that the doping of P can effectually modify the d-band electron density of Pt, leading to a significantly improved electrocatalytic activity. Moreover, the abundant atomic steps/corners as active sites deriving from the unique dendritic structures also contribute to the improved performance. Importantly, this work is expected to provide a versatile approach to the synthesis of other P-doped dendritic metallic alloy with promising energy catalytic applications.

The work was financially supported by NSFC (No. 21373149).

Notes and references

- (a) D. F. van der Vliet, C. Wang, D. Tripkovic, D. Strmcnik, X. F. Zhang, M. K. Debe, R. T. Atanasoski, N. M. Markovic and V. R. Stamenkovic, *Nat. Mat.*, 2012, **11**, 1051-1058; (b) H. Liu, Y. Zheng, G. Wang and S. Z. Qiao, *Adv. Energy Mater.*, 2014, DOI: 10.1002/aenm.201401186.
- (a) W. Chen and S. Chen, *J. Mater. Chem.*, 2011, **21**, 9169-9178; (b) L. Li, L. Hu, J. Li and Z. Wei, *Nano Res.*, 2014, **8**, 418-440; (c) H. Zhang, C.-D. Gu, M.-L. Huang, X.-L. Wang and J.-P. Tu, *Electrochem. Commun.*, 2013, **35**, 108-111.
- (a) A. B. A. Nassr, I. Sinev, M.-M. Pohl, W. Grünert and M. Bron, *ACS Catal.*, 2014, **4**, 2449-2462; (b) X. Yu and P. G. Pickup, *J. Power Sources*, 2008, **182**, 124-132; (c) A. K. Singh and Q. Xu, *ChemCatChem*, 2013, **5**, 652-676; (d) F. Saleem, Z. Zhang, B. Xu, X. Xu, P. He and X. Wang, *J. Am. Chem. Soc.*, 2013, **135**, 18304-18307; (e) R. Wang, J. Liu, P. Liu, X. Bi, X. Yan, W. Wang, Y. Meng, X. Ge, M. Chen and Y. Ding, *Nano Res.*, 2014, **7**, 1569-1580.
- (a) Y. Xu and B. Zhang, *Chem. Soc. Rev.*, 2014, **43**, 2439; (b) X. Zhao, M. Yin, L. Ma, L. Liang, C. Liu, J. Liao, T. Lu and W. Xing, *Energy Environ. Sci.*, 2011, **4**, 2736-2753; (c) L. Ruan, E. Zhu, Y. Chen, Z. Lin, X. Huang, X. Duan and Y. Huang, *Angew. Chem. Int. Ed.*, 2013, **52**, 12577-12581; (d) W. Liu, A.-K. Herrmann, N. C. Bigall, P. Rodriguez, D. Wen, M. Oezaslan, T. J. Schmidt, N. Gaponik and A. Eychmüller, *Acc. Chem. Res.*, 2015, DOI: 10.1021/ar500237c; (e) N. Kakati, J. Maiti, S. H. Lee, S. H. Jee, B. Viswanathan and Y. S. Yoon, *Chem. Rev.*, 2014, **114**, 12397-12429; (f) K. Jiang, H.-X. Zhang, S. Zou and W.-B. Cai, *Phys. Chem. Chem. Phys.*, 2014, **16**, 20360-20376.
- (a) X. Huang, E. Zhu, Y. Chen, Y. Li, C. Y. Chiu, Y. Xu, Z. Lin, X. Duan and Y. Huang, *Adv. Mater.*, 2013, **25**, 2974-2979; (b) J. Gu, Y.-W. Zhang and F. Tao, *Chem. Soc. Rev.*, 2012, **41**, 8050-8065.
- (a) S. Guo, S. Zhang, D. Su and S. Sun, *J. Am. Chem. Soc.*, 2013, **135**, 13879-13884; (b) X. Yu, D. Wang, Q. Peng and Y. Li, *Chem. Eur. J.*, 2013, **19**, 233-239; (c) L. Chen, H. Guo, T. Fujita, A. Hirata, W. Zhang, A. Inoue and M. Chen, *Adv. Funct. Mater.*, 2011, **21**, 4364-4370; (d) Z. Cui, H. Chen, M. Zhao, D. Marshall, Y. Yu, H. Abruña and F. J. DiSalvo, *J. Am. Chem. Soc.*, 2014, **136**, 10206-10209; (e) C. Baldizzone, S. Mezzavilla, H. W. Carvalho, J. C. Meier, A. K. Schuppert, M. Heggen, C. Galeano, J. D. Grunwaldt, F. Schüth and K. J. Mayrhofer, *Angew. Chem. Int. Ed.*, 2014, **53**, 14250-14254; (f) B. Y. Xia, H. B. Wu, N. Li, Y. Yan, X. W. Lou and X. Wang, *Angew. Chem. Int. Ed.*, 2015, DOI: 10.1002/anie.201411544; (g) C. Wang, M. Chi, D. Li, D. Strmcnik, D. van der Vliet, G. Wang, V. Komanicky, K.-C. Chang, A. P. Paulikas, D. Tripkovic, J. Pearson, K. L. More, N. M. Markovic and V. R. Stamenkovic, *J. Am. Chem. Soc.*, 2011, **133**, 14396-14403; (h) Q.-L. Zhu, D.-C. Zhong, U. B. Demirci and Q. Xu, *ACS Catal.*, 2014, **4**, 4261-4268; (i) J. Zhang and C. M. Li, *Chem. Soc. Rev.*, 2012, **41**, 7016-7031.
- (a) M.-L. Lin, M.-Y. Lo and C.-Y. Mou, *Catal. Today*, 2011, **160**, 109-115; (b) A. F. Shao, Z. B. Wang, Y. Y. Chu, Z. Z. Jiang, G. P. Yin and Y. Liu, *Fuel Cells*, 2010, **10**, 472-477; (c) J. Zhang, Y. Xu and B. Zhang, *Chem. Commun.*, 2014, **50**, 13451-13453; (d) L. Zhang, D. Lu, Y. Chen, Y. Tang and T. Lu, *J. Mater. Chem. A*, 2014, **2**, 1252-1256; (e) L. Shang, F. Zhao and B. Zeng, *Int. J. Electrochem. Sci.*, 2015, **10**, 786-794; (f) Y. Y. Tong, C. D. Gu, J. L. Zhang, M. L. Huang, H. Tang, X. L. Wang and J. P. T. ab, *J. Mater. Chem. A*, 2015, **3**, 4669-4678; (g) T. Y. Ma, J. Ran, S. Dai, M. Jaroniec and S. Z. Qiao, *Angew. Chem. Int. Ed.*, 2015, **54**, 4646-4650.
- (a) M. Carmo, R. C. Sekol, S. Ding, G. Kumar, J. Schroers and A. D. Taylor, *ACS Nano*, 2011, **5**, 2979-2983; (b) R. Wang, Y. Ma, H. Wang, J. Key and S. Ji, *Chem. Commun.*, 2014, **50**, 12877-12879.
- (a) X. Xu, X. Zhang, H. Sun, Y. Yang, X. Dai, J. Gao, X. Li, P. Zhang, H. H. Wang, N. F. Yu and S. Sun, *Angew. Chem. Int. Ed.*, 2014, **126**, 12730-12735; (b) B. Y. Xia, H. B. Wu, X. Wang and X. W. Lou, *Angew. Chem. Int. Ed.*, 2013, **52**, 12337-12340; (c) H. Lee, S. E. Habas, S. Kweskin, D. Butcher, G. A. Somorjai and P. Yang, *Angew. Chem. Int. Ed.*, 2006, **45**, 7824-7828; (d) C. Li, T. Sato and Y. Yamauchi, *Angew. Chem. Int. Ed.*, 2013, **52**, 8050-8053; (e) C. J. DeSantis, A. C. Sue, M. M. Bower and S. E. Skrabalak, *ACS Nano*, 2012, **6**, 2617-2628; (f) M. Chen, B. Wu, J. Yang and N. Zheng, *Adv. Mater.*, 2012, **24**, 862-879; (g) J. Zhang, H. Yang, J. Fang and S. Zou, *Nano Lett.*, 2010, **10**, 638-644; (h) N. S. Porter, H. Wu, Z. Quan and J. Fang, *Acc. Chem. Res.*, 2013, **46**, 1867-1877; (i) Y. Bing, H. Liu, L. Zhang, D. Ghosh and J. Zhang, *Chem. Soc. Rev.*, 2010, **39**, 2184-2202.
- (a) B. Lim and Y. Xia, *Angew. Chem. Int. Ed.*, 2011, **50**, 76-85; (b) L. Wang and Y. Yamauchi, *J. Am. Chem. Soc.*, 2009, **131**, 9152-9153; (c) L. Wang and Y. Yamauchi, *J. Am. Chem. Soc.*, 2013, **135**, 16762-16765.
- (a) S. Sun, G. Zhang, D. Geng, Y. Chen, R. Li, M. Cai and X. Sun, *Angew. Chem. Int. Ed.*, 2011, **50**, 422-426; (b) E. Taylor, S. Chen, J. Tao, L. Wu, Y. Zhu and J. Chen, *ChemSusChem*, 2013, **6**, 1863-1867; (c) W. Wang, D. Wang, X. Liu, Q. Peng and Y. Li, *Chem. Commun.*, 2013, **49**, 2903-2905; (d) D.-B. Huang, Q. Yuan, H.-H. Wang and Z.-Y. Zhou, *Chem. Commun.*, 2014, **50**, 13551-13554; (e) F. Wang, C. Li, L.-D. Sun, C.-H. Xu, J. Wang, J. C. Yu and C.-H. Yan, *Angew. Chem. Int. Ed.*, 2012, **51**, 4872-4876.
- (a) Y. Li, W. Ding, M. Li, H. Xia, D. Wang and X. Tao, *J. Mater. Chem. A*, 2015, **3**, 368-376; (b) J. Wu and H. Yang, *Acc. Chem. Res.*, 2013, **46**, 1848-1857.
- H. Liu, C. Koenigsmann, R. R. Adzic and S. S. Wong, *ACS Catal.*, 2014, **4**, 2544-2555.
- R. Jiang, D. T. Tran, J. P. McClure and D. Chu, *ACS Catal.*, 2014, **4**, 2577-2586.
- (a) J. Chang, L. Feng, C. Liu, W. Xing and X. Hu, *Energy Environ. Sci.*, 2014, **7**, 1628-1632; (b) S. Chen, H. Su, Y. Wang, W. Wu and J. Zeng, *Angew. Chem. Int. Ed.*, 2015, **54**, 108-113; (c) H. Huang, S. Yang, R. Vajtai, X. Wang and P. M. Ajayan, *Adv. Mater.*, 2014, **26**, 5160-5165.
- L. X. Ding, A. L. Wang, G. R. Li, Z. Q. Liu, W. X. Zhao, C. Y. Su and Y. X. Tong, *J. Am. Chem. Soc.*, 2012, **134**, 5730-5733.
- D. F. van der Vliet, C. Wang, D. Li, A. P. Paulikas, J. Greeley, R. B. Rankin, D. Strmcnik, D. Tripkovic, N. M. Markovic and V. R. Stamenkovic, *Angew. Chem. Int. Ed.*, 2012, **124**, 3193-3196.
- M. E. Scofield, C. Koenigsmann, L. Wang, H. Liu and S. S. Wong, *Energy Environ. Sci.*, 2015, **8**, 350-363.
- Q. Chen, J. Zhang, Y. Jia, Z. Jiang, Z. Xie and L. Zheng, *Nanoscale*, 2014, **6**, 7019-7024.
- Y. Ma, R. Wang, H. Wang, V. Linkov and S. Ji, *Phys. Chem. Chem. Phys.*, 2014, **16**, 3593-3602.